

CERN-TH-2026-032, Nikhef 2026-005, OUTP-26-02P

A generalised- k_t jet algorithm for Deep Inelastic Scattering

Melissa van Beekveld¹, Silvia Ferrario Ravasio², Alexander Karlberg^{3,4}, Darcy Peake⁵¹ Nikhef, Theory Group, Science Park 105, 1098 XG, Amsterdam, The Netherlands² Dipartimento di Fisica, Università di Torino, and INFN, Sezione di Torino, Via P. Giuria 1, I-10125 Torino, Italy³ Rudolf Peierls Centre for Theoretical Physics, Clarendon Laboratory, Parks Road, University of Oxford, Oxford OX1 3PU, UK⁴ CERN, Theoretical Physics Department, CH-1211 Geneva 23, Switzerland⁵ Department of Physics and Astronomy, University of Sussex, Sussex House, Brighton, BN1 9RH, UK

mbeekvel@nikhef.nl, silvia.ferrario Ravasio@unito.it, alexander.karlberg@cern.ch, n.peake@sussex.ac.uk

Abstract

We introduce an inclusive generalised- k_t jet algorithm for Deep Inelastic Scattering, defined in the Breit frame and implemented in `fjcontrib`. The family of algorithms is governed by the usual parameter p , which controls the transverse-momentum dependence of the algorithm, as well as by a jet radius parameter R . The angular-ordered ($p = 0$) version of the algorithm was already presented by some of us, and can be used to formulate observables with simple all-order structures. In this article we investigate phenomenological applications of the algorithms related to the identification of the jet associated with the struck quark, and assess their sensitivity to non-perturbative effects, such as hadronisation. We also perform comparisons with the recent Centauro algorithm.

The code is available from <https://fastjet.fr/contrib/> as the plugin `DISGenkt`.

Copyright attribution to authors.

This work is a submission to SciPost Phys. Comm. Rep.

License information to appear upon publication.

Publication information to appear upon publication.

Received Date

Accepted Date

Published Date

Contents

1	Introduction	2
2	DIS kinematics and the Breit Frame	4
3	Existing DIS jet algorithms	4
3.1	Exclusive jet algorithms for e^+e^- collisions	5
3.1.1	The Durham jet algorithm	5
3.1.2	The Cambridge jet algorithm	5
3.2	Exclusive jet algorithms for DIS collisions	6
3.2.1	Exclusive k_t -algorithm for DIS	6
3.2.2	Cambridge algorithm for DIS	6
3.3	Generalised inclusive k_t -algorithms for DIS	7
3.4	Centauro algorithm	8
4	A generalised-k_t algorithm for DIS	9
4.1	The algorithm	9
4.2	Identifying the macrojet	10
5	Phenomenological results	11
5.1	Properties of the reconstructed jets	12
5.2	Macrojet observables at hadron level	14
5.3	Impact of hadronisation and beam remnants	16
6	Conclusion	17
	References	18

1 Introduction

Lepton-hadron colliders such as the Hadron Elektron Ringanlage (HERA) and the forthcoming Electron–Ion Collider (EIC) are unique laboratories for the clean investigation of the inner structure of the nucleons and the nuclei that they form. Although the HERA collider has not been operational since 2007, access to previously recorded HERA data has enabled recent re-analyses taking advantage of modern jet algorithms and event-shape observables in Deep Inelastic Scattering (DIS) [1–6]. In the theory community this has spurred a renewed interest in formulating jet algorithms [7–9], and in performing resummed calculations of event shapes for DIS [10–15], the latter building upon earlier work (see e.g. Refs. [16–21]). Such modern QCD tools will be instrumental for the EIC,¹ currently under construction at Brookhaven National Laboratory, whose operation is scheduled to start in the early 2030s. The EIC will provide new opportunities to study the structure of QCD, including the spin structure of the proton, the dynamics of confinement, and gluon saturation [23, 24]. Since jet production is the dominant process at hadron-lepton colliders,

¹And the LHeC [22] should it be approved.

jet reconstruction will play an essential part in many (re)-analyses for both the EIC and HERA.

Most developments in jet algorithms over the past decades have been driven by hadron collider applications, in particular at the LHC, where the anti- k_t algorithm [25] has become the standard choice. Jet algorithms for DIS were developed around the same time as those for hadronic collisions, but unlike for hadron collisions, no single algorithm dominates the landscape. The exclusive (spherically-invariant) k_t algorithm was introduced in Ref. [26] extending the Durham algorithm for e^+e^- collisions [27, 28] to DIS by treating the proton remnant as a particle of infinite momentum. An angular-ordered version of this algorithm was later proposed in Ref. [29]. It modifies the e^+e^- Cambridge algorithm [30] to DIS again by treating the proton remnant as a particle of infinite momentum. A longitudinally invariant (LI) k_t algorithm was introduced in Ref. [31, 32], and was extended to an angular-ordered version (the Aachen algorithm) in Ref. [29]. The latter two algorithms are identical to the hadron-collider versions, except that the clustering takes place in the Breit frame as is the case for all the DIS jet algorithms listed here (cf. Sec. 2 for details on the Breit frame). More recently, the Centauro algorithm [7] was proposed, combining features of longitudinally-invariant k_t algorithms with those of spherically-invariant algorithms. Likewise a set of jet definitions suitable for small- x_B DIS were proposed in Ref. [9]. Most of the historical algorithms, including a modified version of the JADE algorithm [33, 34], have been studied extensively at HERA and Fermilab's E665 experiment [35–52], highlighting the importance of jet finding algorithms in DIS. The recent Centauro algorithm has also recently been used by the H1 collaboration to perform the first measurement of groomed event shapes [6] in DIS.

Unlike at the LHC, where one of the main requirements of a good jet algorithm is the insensitivity to pile-up and underlying event, in DIS, where these effects are suppressed, a good jet algorithm is one that preserves a meaningful clustering sequence and allows soft radiation to influence jet boundaries while respecting the natural hemisphere structure of the Breit frame. For this reason it is natural to consider k_t and Cambridge/Aachen (C/A) type algorithms in DIS, in addition to anti- k_t . A C/A-based DIS algorithm designed for the study of Lund variables [15, 53] and parton shower logarithmic accuracy was introduced in Ref. [8], and forms the starting point for an inclusive generalised- k_t algorithm adapted to DIS, which we present and study in more detail in the present paper. The formulation of the jet algorithm itself follows the structure of the generalised- k_t algorithm used in e^+e^- collisions as implemented and introduced in **Fastjet** [54], but is formulated in the Breit frame and uses a beam distance that is sensitive to the angular separation between the proton and the particles taking part in the clustering. We also discuss a prescription to select the jet that is most likely to contain the struck quark based on the lightcone fraction that the jet is carrying. This allows for a clean separation between *target* and *current* hemisphere jets. Finally, we study the robustness of the new jet algorithm against hadronisation corrections.

The structure of this paper is as follows. In Section 2 we introduce the kinematics relevant to DIS and define the Breit frame. In Section 3 we summarise historical DIS jet algorithms and the recently proposed Centauro one, while in Section 4 we present our new inclusive generalised- k_t jet algorithm. In Section 5 we examine the behaviour of the new algorithms and we provide a comparison with the Centauro one. Finally, we present our conclusions in Section 6.

2 DIS kinematics and the Breit Frame

The DIS process is defined by the partonic scattering process

$$\ell_i(k) + h(P) \rightarrow \ell'_f(k') + X, \quad (1)$$

where P^μ is the momentum of the incoming nucleon h , k^μ is the momentum of the lepton beam ℓ_i , k'^μ is the momentum of the outgoing lepton ℓ'_f , and X denotes the hadronic final state. The standard DIS invariants are

$$Q^2 = -q^2, \quad x_B = \frac{Q^2}{2P \cdot q}, \quad y_{\text{DIS}} = \frac{P \cdot q}{P \cdot k}, \quad (2)$$

with $q^\mu = k^\mu - k'^\mu$ the momentum of the exchanged virtual photon. At the lowest perturbative order, the hadronic final state consists of a single outgoing parton,

$$\ell_i(k) + p_{\text{in}} \rightarrow \ell_f(k') + p_{\text{out}}, \quad (3)$$

where $p_{\text{in}}^\mu = x_B P^\mu$ and $p_{\text{out}}^\mu = q^\mu + p_{\text{in}}^\mu$ are the momenta of the incoming and outgoing partons, respectively. The *Breit frame* plays a central role in many DIS jet algorithms [55].² It is defined by

$$2x_B \vec{P} + \vec{q} = 0, \quad (4)$$

such that the virtual photon carries no energy component and is aligned along the z -axis, i.e.

$$q^\mu = (0, 0, 0, -Q), \quad (5)$$

and is therefore purely space-like. In this frame, the incoming and outgoing parton momenta take the simple form

$$p_{\text{in}}^\mu = \frac{Q}{2}(1, 0, 0, +1), \quad p_{\text{out}}^\mu = \frac{Q}{2}(1, 0, 0, -1). \quad (6)$$

Thus, the proton and virtual photon collide head-on in the Breit frame. Within this frame, the proton remnant appears in the region at positive rapidity (generally referred to as the *target hemisphere*), while the struck quark lies in the negative rapidity region (the *current hemisphere*). In practice, the jet clustering in this frame can lead to radiation from the proton remnant being absorbed into the struck-quark jet, making the separation between the two hemispheres an important feature of DIS jet algorithms.

3 Existing DIS jet algorithms

Before presenting a generalised- k_t algorithm for DIS in Section 4, it is instructive to first discuss existing jet algorithms that have historically been used for DIS, focusing on sequential-recombination jet algorithms. The overview we present here serves to explain how jet algorithms are formulated in general, but will also allow us to highlight similarities and differences between existing jet algorithms and the new generalised k_t jet algorithm for DIS. We formulate the jet algorithms in the Breit frame, but note that those algorithms that are longitudinally boost invariant, such as Centauro and some of the inclusive k_t -algorithms (cf. Secs. 3.3 and 3.4), can also be formulated in a frame that is connected to the Breit frame through a longitudinal boost.³

²The frame was first introduced in Ref. [56] in the context of relativistic scattering kinematics. The term ‘Breit frame’ was first coined by Ernst, Sachs, and Wali in Refs. [57, 58]. For an explicit implementation we refer the reader to Appendix 7.11 in Ref. [59].

³We note that the lab frame in DIS is *not* connected to the Breit frame through only a longitudinal boost, but requires a rotation as well.

3.1 Exclusive jet algorithms for e^+e^- collisions

Since some of the existing DIS jet algorithms are adapted from their e^+e^- counterparts, and in fact use e^+e^- clustering explicitly in a re-clustering step, we start by reviewing the e^+e^- variants before turning to DIS.

3.1.1 The Durham jet algorithm

The Durham algorithm was introduced in Ref. [27,28]. Given a list of objects undergoing the clustering procedure, which are conventionally called pseudojets, one introduces a dimensionless resolution parameter y_{ij} that reads

$$y_{ij} = \frac{\min(E_i^2, E_j^2)}{s} 2(1 - \cos \theta_{ij}), \quad (7)$$

with E_i, E_j the energies of the two pseudojets, θ_{ij} the angle between them, and \sqrt{s} the center-of-mass energy of the collision. One also introduces a parameter $y_{\text{cut}} \leq 1$. The algorithm then proceeds as follows.

1. For every pair of pseudojets compute y_{ij} .
2. The pair with the smallest y_{ij} is clustered together if $y_{ij} < y_{\text{cut}}$, meaning that a pseudojet with momentum $p_{ij} = p_i + p_j$ is inserted in the list of pseudojets, which replaces i and j .⁴
3. Repeat from 1 until all $y_{ij} \geq y_{\text{cut}}$ at which point the remaining pseudo-jets are identified as jets.

After the clustering terminates, each particle in the event is either merged into a jet, or it remains as a single-particle jet, making it an exclusive algorithm.

3.1.2 The Cambridge jet algorithm

The Cambridge algorithm, introduced in Ref. [30], differs from the Durham algorithm by introducing, next to a merging condition, also a distance measure d_{ij} , which reads

$$d_{ij} = 2(1 - \cos \theta_{ij}). \quad (8)$$

This choice was motivated by the aim of producing a clustering sequence that closely follows the coherent pattern of QCD radiation, where a possible merging of two partons that are close in angle is considered before the possible merge of two particles that are more widely separated. The merging of two particles is decided on the Durham distance measure y_{ij} . Secondly, the clustering algorithm itself is modified with a ‘soft freezing’ mechanism, which prevents the softer of two pseudojets to attract any additional pseudojets. The Cambridge algorithm proceeds as follows.

1. Compute d_{ij} for all pairs and select the pair of pseudojets with the smallest d_{ij} .
2. For this pair, if $y_{ij} < y_{\text{cut}}$, delete i and j and introduce a new pseudojet with momentum $p_{ij} = p_i + p_j$. If instead $y_{ij} \geq y_{\text{cut}}$, the softer (i.e. less energetic) pseudojet is removed from the list and is promoted to a jet: this mechanism is called soft freezing.
3. Repeat from 1 until there are no more pseudojets to be clustered.

The last pseudojet that remains in the list of pseudojets is also promoted to a jet.

⁴This recombination is dubbed the E -scheme but other alternatives exist [27,33,34].

3.2 Exclusive jet algorithms for DIS collisions

3.2.1 Exclusive k_t -algorithm for DIS

The exclusive k_t -algorithm for DIS was presented in Ref. [26]. It is based on the equivalent e^+e^- variant [27] that we discussed above, but treats also the additional initial-state (and beam remnant) collinear singularities. The algorithm is formulated in the Breit frame. Instead of using the center-of-mass energy \sqrt{s} , one introduces a transverse-momentum-like scale E_t satisfying $\Lambda \ll E_t \leq Q$ and defines a resolution variable y_{ij} between two pseudojets as

$$y_{ij} = \frac{\min(E_i^2, E_j^2)}{E_t^2} 2(1 - \cos \theta_{ij}), \quad (9)$$

as well as a beam resolution parameter for each pseudojet

$$y_{iB} = \frac{E_i^2}{E_t^2} 2(1 - \cos \theta_{iB}), \quad (10)$$

where θ_{ij} is the angular separation between two pseudojets, θ_{iB} is the angle of pseudojet i with respect to the beam, and E_i and E_j are the energies of the corresponding pseudojets. The E_t variable determines how close to the beam direction (in the Breit frame) resulting jets are allowed to be formed, with the transverse momentum of the resulting jets satisfying $p_t > E_t$. The clustering procedure works in two steps. In the first step, a pre-clustering takes place, with the aim of separating particles into a *beam* and a set of *macro-jets*, and operates as follows.

1. For every pseudojet i compute y_{iB} and for every pair i, j compute y_{ij} .
2. Take the smallest value of all y_{ij} and y_{iB} . If the smallest value is a y_{ij} and $y_{ij} < 1$, combine their momenta into a new pseudojet. If $y_{iB} < 1$ is the smallest, include i into the beam jet, and remove it from the list of pseudojets.
3. Repeat the procedure from step 1 for all pseudojets, until all distance measures are $y_{ij}, y_{iB} > 1$.

The resulting objects that remain at this stage are the final-state macro-jets, and does not include the beam jet. In the second step of the algorithm we resolve the structure of the final-state macro-jets. The input for this second step consists of all the constituents of these jets. At this stage, a resolution parameter $y_{\text{cut}} = Q_0^2/E_t^2 < 1$ is introduced, with $Q_0 < E_t$, and the algorithm proceeds by clustering the constituents using the e^+e^- Durham algorithm (Sec. 3.1.1). The objects that remain at the end are the final-state jets. The full two-step procedure produces jets with relative transverse momenta k_t in the range $\sqrt{y_{\text{cut}}}E_t < k_t < E_t$, and with a Breit-frame transverse momentum $p_t > E_t$. Every particle in the event ends up either in the list of final-state jets or in the beam jet.

3.2.2 Cambridge algorithm for DIS

The Cambridge algorithm for DIS was introduced in Ref. [29]. It is an exclusive algorithm, inspired by the Cambridge algorithm for e^+e^- -collisions [30], and very similar to the exclusive k_t -algorithm presented in Sec. 3.2.1. Like in e^+e^- , one decouples the merging step from the ordering step, now by introducing two distance measures: d_{ij} and d_{iB} , which read

$$d_{ij} = 2(1 - \cos \theta_{ij}), \quad (11)$$

and

$$d_{iB} = 2(1 - \cos \theta_{iB}). \quad (12)$$

Like for the exclusive k_t -algorithm presented in Sec. 3.2.1, also in this case the algorithm proceeds in two steps. The first step is

1. For every pseudojet i compute d_{iB} and for every pair i, j compute d_{ij} .
2. Take the smallest value of all d_{ij} and d_{iB} . If the smallest value is a d_{ij} , combine their momenta into a new pseudojet if $y_{ij} < 1$ otherwise call the softest (less energetic) a jet (i.e. apply the freezing mechanism). If d_{iB} is the smallest include i as a beam jet, and remove it from the list of pseudojets if $y_{iB} < 1$, otherwise promote it to a jet.
3. Repeat the procedure from step 1 for all pseudojets, until all resolution variables $y_{ij}, y_{iB} > 1$, at which point we promote all the remaining pseudojets to jets and proceed with the second step.

In the second step of the algorithm we undo the clustering of all the jets (excluding the beam jet), and re-cluster the constituents using the e^+e^- -Cambridge algorithm using a resolution parameter y_{cut} .

3.3 Generalised inclusive k_t -algorithms for DIS

The jet algorithms for DIS discussed so far were all **exclusive**. For an **inclusive** algorithm, when the smallest distance is the one between the beam(s) and a pseudo-jet, the pseudo-jet is promoted to a jet rather than being absorbed into a beam remnant collection. The total number of jets is therefore an infrared unsafe observable, because it includes jets that can be either very soft or collinear with the beam. Only after introducing a suitable resolution parameter (like a minimum transverse momentum with respect to the beam) and removing jets that fall below this resolution parameter, will it be infrared safe.

The inclusive longitudinally-invariant (LI) k_t -algorithm was first introduced in Ref. [32] (see Ref. [31] for the exclusive version) for hadron-hadron collisions. An angular-ordered variant, often referred to as the Aachen or Cambridge/Aachen algorithm, was since introduced in Ref. [29] and then eventually the family of generalised inclusive k_t -algorithms was introduced in Ref. [25] along with the anti- k_t algorithm. The DIS variant is in this case identical to the hadron-hadron variant, except that the clustering takes place in the Breit frame. We define a set of distance measures d_{ij} and d_{iB} , which are dimensionful for $p \neq 0$, given by

$$d_{ij} = \min(p_{Ti}^{2p}, p_{Tj}^{2p}) \frac{\Delta R_{ij}^2}{R^2}, \quad d_{iB} = p_{Ti}^{2p}, \quad (13)$$

where $\Delta R_{ij}^2 = (y_i - y_j)^2 + (\phi_i - \phi_j)^2$, with y_i the rapidity and ϕ_i the azimuthal angle of pseudojet i . The procedure is then given by

1. Compute all the distances d_{ij} and d_{iB} . If a d_{ij} is the smallest, cluster i and j , if d_{iB} is the smallest call i a jet.
2. Repeat until no more pseudojets remain.

We note that the k_t -algorithm corresponds to $p = 1$, C/A to $p = 0$ and anti- k_t to $p = -1$.

Note that one is not restricted to using distances that are natural for pp collisions. Indeed, the inclusive algorithm can be made spherically invariant (SI) instead of LI, which is more appropriate for e^+e^- collisions [54], by replacing the distance measures with

$$d_{ij} = \min(E_i^{2p}, E_j^{2p}) \frac{1 - \cos \theta_{ij}}{f(R)}, \quad d_{iB} = E_i^{2p}, \quad (14)$$

with

$$f(R) = \begin{cases} 1 - \cos R & 0 < R < \pi \\ 3 + \cos R & \pi < R < 2\pi. \end{cases} \quad (15)$$

In this case, the beam distance d_{iB} is not sensitive to the angular separation between the pseudo-jet i and the beam, but only on the energy of the pseudo-jet. This feature is not desirable in the context of ep collisions, which is an asymmetrical collision, where we need to distinguish between a collinear and an anti-collinear direction, as there is only one hadronic beam.

3.4 Centauro algorithm

The Centauro algorithm [7] is a longitudinally invariant jet algorithm designed to capture jets close to the Born configuration in the Breit frame. Longitudinally invariant k_t -type algorithms such as those presented in Sec. 3.3 cluster in the (y, ϕ) plane and are unable to form a jet along the beam axis, where $y \rightarrow -\infty$. Conversely, the spherically invariant algorithms can cluster around the beam axis but do not preserve longitudinal invariance.

The Centauro algorithm is designed to address both of these aspects. It is built around the variable $\bar{\eta}_i$ that behaves differently in the two hemispheres:

- **Current hemisphere:** $\bar{\eta}_i$ decreases as particles become closer in angle, allowing particles in this hemisphere to cluster.
- **Target hemisphere:** $\bar{\eta}_i$ becomes large and diverges. This prevents clustering in the proton beam region, similar to the behaviour of the anti- k_t -algorithm.

Working in the Breit frame, for every momentum p_i^μ , one defines the variable $\bar{\eta}_i$ as

$$\bar{\eta}_i = -2 \frac{Q}{q \cdot n_{\text{out}}} \frac{p_{T,i}}{p_i \cdot n_{\text{in}}}, \quad (16)$$

with

$$n_{\text{in}}^\mu = \frac{2}{Q} x_B P^\mu \quad (17a)$$

$$n_{\text{out}}^\mu = \frac{2}{Q} (q^\mu + x_B P^\mu) \quad (17b)$$

$$p_{T,i}^2 = \frac{2(p_i \cdot n_{\text{in}})(p_i \cdot n_{\text{out}})}{n_{\text{in}} \cdot n_{\text{out}}}, \quad (17c)$$

meaning that $p_{T,i}$ is the transverse component of the momentum in the Breit frame (or any other frame that only differs by a longitudinal boost from the Breit frame). From this, one constructs the inter-pseudojet distance measure as ⁵

$$d_{ij} = \frac{(\bar{\eta}_i - \bar{\eta}_j)^2 + 2\bar{\eta}_i \bar{\eta}_j (1 - \cos \Delta\phi_{ij})}{R^2}. \quad (18)$$

The distance to the beam is always equal to $d_{iB} = 1$. One then clusters jets according to the procedure given in Sec. 3.3.

⁵Note that we are reporting the definition used in the `fjcontrib` implementation, which is the one we have also used in this work.

4 A generalised- k_t algorithm for DIS

4.1 The algorithm

We now introduce a generalised- k_t algorithm for DIS, implemented as a FASTJET plugin in `fjcontrib`. The algorithm shares the essential structure of its e^+e^- counterpart, introduced at the end of Sec. 3.3, with the key modification that the beam distance is now sensitive to the angular separation with respect to the proton beam and the clustering takes place in the Breit frame. The angular-ordered variant of the algorithm ($p = 0$) was already presented by some of us in Ref. [8], and used to define Lund Tree Event shapes with remarkably simple all-orders structure [15]. Here we present the extension for $p \neq 0$, and include two parameters, R and y_{cut} (to be detailed below), that control the behaviour of the algorithm. We first define the distances

$$d_{ij} = \min(E_i^{2p}, E_j^{2p}) \frac{(1 - \cos \theta_{ij})}{1 - \cos R}, \quad (19a)$$

$$d_{iB} = E_i^{2p} (1 - \cos \theta_{iB}), \quad (19b)$$

where $R < \pi$. The algorithm is then as follows.

1. Compute all d_{ij} and d_{iB} . If the smallest is a d_{iB} , call i a jet, and remove it from the list of pseudojets. If the smallest is a d_{ij} , cluster i and j .
2. Continue until there are no pseudojets left in the list.

The introduction of the distance d_{iB} measuring both the energy and the closeness in angle to the beam direction, allows one to cluster jets in the current hemisphere while promoting remnant hemisphere particles to jets early in the cluster sequence. Note that the C/A variant ($p = 0$) presented in Ref. [8] uses $R = \frac{\pi}{2}$.⁶ For $p = 0$, the energy of a particle does not enter the distance measure, and particles are merged purely based on angular proximity. For $p = 1$, i.e. the k_t variant of the algorithm, soft particles typically lead to smaller d_{ij} and therefore are clustered first. On the contrary, for $p = -1$, i.e. the anti- k_t variant, hard final-state particles will cluster first.

As in the standard inclusive (LI) algorithms for pp collisions, some reconstructed jets may originate entirely from initial-state radiation or from soft large-angle emissions. In pp collisions, such jets are removed by imposing a transverse-momentum (and a rapidity) cut. This however cannot be applied to DIS, as the jet originating from the fragmentation of the struck quark does not necessarily carry a large transverse momentum (in fact, in the case where no additional radiation is produced, this jet will carry zero transverse momentum). To remove only soft jets or jets collinear to the beam, one can define an ordering variable according to the (scaled) effective transverse momentum

$$y_{iB} = 2 \frac{E_i^2}{Q^2} (1 - \cos \theta_{iB}), \quad (20)$$

and discard jets with $y_{iB} < y_{\text{cut}}$. Alternatively, one might use an ordering variable based on the light-cone fraction of the original struck-quark momentum carried by the i^{th} jet, defined by

$$z_i = \frac{2x_B p_i \cdot P}{Q^2} = 2 \frac{E_i}{Q} (1 - \cos \theta_{iB}), \quad (21)$$

⁶It is also possible to formulate an exclusive variant of our algorithm by introducing a dimensionless quantity y_{ij} and an associated y_{cut} . The $p = 0$ zero variant will then share some similarities with the algorithm in Sec. 3.2.2 but without the final re-clustering step. We do not explore this variant any further in this paper.

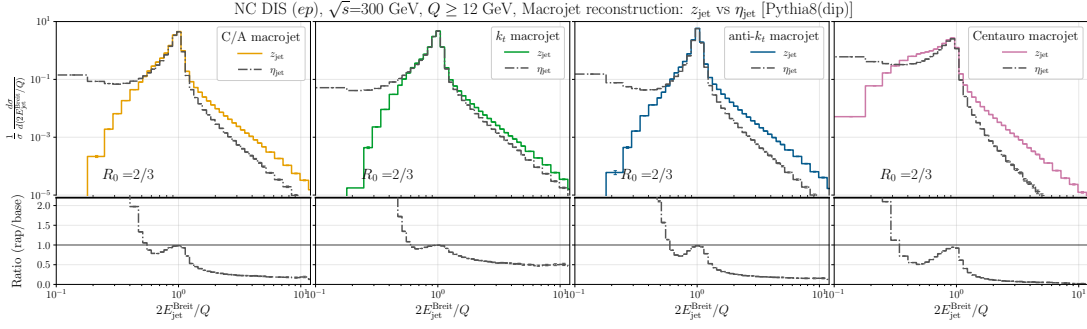


Figure 1: Normalised Breit-frame energy distribution of the final-state macrojet for neutral-current DIS, $\sqrt{s}=300$ GeV using, from left to right, the inclusive version of the generalised k_t algorithms with $R_0 = 2/3$ and $p = 0$ (C/A), 1 (k_t), and $p = -1$ (anti- k_t), followed by the Centauro jet algorithm with $R_0 = 2/3$. The final-state macrojet is identified as the one that maximises the light-cone component opposite in direction to the proton (z_{jet} , solid line) or the Breit-frame pseudo-rapidity (η_{jet} , dash-dotted lines). Events are generated using the Pythia 8.3 [60] default shower, with dipole recoil option [61]. See Tab. 1 for further settings.

where P is the proton momentum. One may then discard jets with $z_i < z_{\text{cut}}$, with $0 < z_{\text{cut}} < 1$. Below, we discuss how to use z_i to select what we will call the *macrojet*. Differences between Centauro (Sec. 3.4) and the generalised- k_t jet algorithm presented here will be explored in Sec. 5.

4.2 Identifying the macrojet

This section describes how we identify the *final-state macrojet*, defined as the jet that is most likely to contain the fragments of the struck quark. Our prescription is to select the jet that carries the largest light-cone component z_{jet} along the direction of the original struck quark. To make this precise, we perform a Sudakov decomposition of each jet momentum (see also Sec. 2 and Ref. [10])

$$p_{\text{jet}}^\mu = p_{\text{jet}}^- x_B P^\mu + z_{\text{jet}} p_{\text{out}}^\mu + k_\perp^\mu, \quad (22)$$

where P^μ is the proton momentum, and as before, $p_{\text{out}}^\mu = q^\mu + x_B P^\mu$ is the original struck-quark momentum. The coefficient p_{jet}^- is given by

$$p_{\text{jet}}^- = \frac{|\vec{k}_\perp|^2 + p_{\text{jet}}^2}{Q^2 z_{\text{jet}}}. \quad (23)$$

The vector k_\perp^μ is a space-like vector orthogonal to P^μ and p_{out}^μ .⁷ Maximising z_{jet} is then equivalent to selecting the jet whose momentum p_{jet}^μ has the largest dot product with P^μ . As discussed in Ref. [8], this prescription is infrared safe. A seemingly natural alternative is to identify the macrojet as the jet with the most negative rapidity. However, this prescription is not infrared safe, as illustrated in Fig. 1. There, one can observe that both for the new family of jet algorithms introduced here and for the Centauro jet algorithm, identifying the final-state macrojet by rapidity (dash-dotted lines) leads to a soft tail. This tail is produced by wrongfully identifying soft emissions, generated either

⁷Note that in Eq. (22) we have adopted the notation of Ref. [10] to label the lightcone component along the proton in the ‘-’ direction.

Input Parameter	Value
PDF	NNPDF40MC_nlo_as_01180
\sqrt{s}	300 GeV
Q_{\min}	12 GeV
Hadronisation effects	On
Beam remnants	On
QED	Off
Tune	Monash [63]

Table 1: Input parameters used for the numerical results presented below.

from radiation off the DIS hard-scattering process or from the beam remnant, as the final-state macrojet. This means that selecting the jet with the most negative rapidity is not infrared safe because an arbitrarily soft emission at sufficiently negative rapidity can alter the jet assignment discontinuously. We note that for the k_t -algorithm the soft tail is partially suppressed even when selecting the macrojet with the most negative rapidity, but there is no exponential decrease in the tail. Maximising the light-cone component in the direction of the original struck quark (solid curves) exponentially suppresses the tail for all algorithms.

Beyond macrojet identification, the properties of the macrojet itself provide a useful way to characterise the behaviour of the algorithm. In particular, the macrojet offers a direct handle separating the remnant hemisphere from the current hemisphere. We will explore this further in the next section.

We conclude this section by explicitly discussing the infrared and collinear safety of the jet algorithm and the macrojet definition. In the Born limit, the only final-state parton lies in the current hemisphere and is promoted to a single jet with $z_{\text{jet}} = 1$, so that the macrojet prescription reproduces the struck-quark direction. Collinear splittings are clustered by the recombination step before they can affect the resolved jet structure, and the macrojet selection remains unchanged because z_{jet} is additive under such splittings, preserving the total light-cone momentum of the parent jet. Soft emissions either cluster with a nearby hard pseudojet or form separate soft jets whose light-cone fraction vanishes in the soft limit. They therefore cannot change the largest- z_{jet} assignment except in degenerate configurations of measure zero. The resolved macrojet observables considered below are consequently insensitive to arbitrarily soft emissions and collinear splittings.

5 Phenomenological results

In this section we explore a few macrojet distributions obtained with our inclusive jet algorithms. In what follows we will simply label the $p = -1$ variant of the algorithm with anti- k_t , $p = 0$ with C/A, and $p = 1$ with k_t . We compare them to the Centauro algorithm to highlight differences and similarities.

DIS neutral-current events are produced using the `Pythia 8.3` [60] event generator, with the native `Pythia` shower with dipole local recoil [61]. The analysis is performed with `RIVET 3.1.8` [62]. The parameters, unless otherwise stated, used for the results presented in the following sections are summarised in Table 1. In Sec. 5.1 we investigate the properties of all the reconstructed jets, while in Sec. 5.2 and 5.3 we focus on the final-state macrojet distributions.

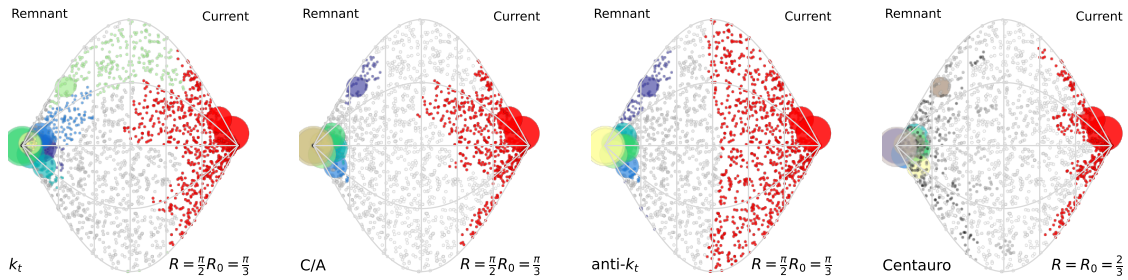


Figure 2: From left to right, we show the jet and jet boundaries for the k_t ($p = 1$), C/A ($p = 0$), anti- k_t ($p = -1$) and Centauro jet algorithms for a DIS event with $x_B = 0.2$ and $Q = 114$ GeV. Each particle is represented by a disc whose area is proportional to its energy, while its position corresponds to the direction of its momentum projected onto the unfolded sphere around the hard-scattering vertex. In addition to the physical particles, we have added a sea of 2000 ghosts [64] to better illustrate how the shape of the jet boundaries. The soft particles that are not part of any physical jet are coloured gray. Vertical lines indicate constant θ , and curved lines indicate constant ϕ . The remnant hemisphere lies in the left half of the plot and the current hemisphere in the right half of the plot. All particles clustered into a given jet share the same color, and jets only made out of ghost particles are coloured gray. Particles entering the final-state macro-jet are highlighted in red.

5.1 Properties of the reconstructed jets

To better understand general features of the new jet algorithms and how they compare to the Centauro jet algorithm, we show in Fig. 2 the (θ, ϕ) distribution of particles from a DIS event obtained after showering (but before hadronisation). The location of the central point in each disc corresponds to the particle's position in the θ and ϕ plane, while the size of the disc illustrates the particle's energy, with larger radii corresponding to higher relative energies. Particles in the remnant hemisphere lie on the left-hand side of each figure, while particles in the current hemisphere lie on the right-hand side. Particles entering the same jet share the same colour. Those forming the final-state macrojet are coloured in red. We have placed the event in a sea of 2000 additional ultra-soft particles, dubbed ghosts in Ref. [64], where the idea of illustrating the jet boundaries was originally introduced. We generate these ghosts with a fixed energy ($E = 10^{-6}$ GeV) and with a uniform distribution in θ and ϕ . We stress here that the exact shape of the jet boundaries depends to some extent on the exact distribution of the soft particles.

Upon inspection of Fig. 2, one of the most striking visual features is that of the jet boundary produced by the anti- k_t algorithm. We see that the jet boundary for the final-state macrojet in this case follows the lines of constant θ . This is a direct consequence of the anti- k_t clustering sequence, which always initiates clustering from the hardest particle outward, producing perfectly conical jets in the θ, ϕ plane. This circular symmetry is not shared by the other algorithms: k_t , C/A and Centauro all produce jets with irregular, jagged boundaries.

Following Ref. [7], we adopt

$$R_{\text{generalised-}k_t} = \frac{\pi}{2} R_{\text{centauro}} \equiv \frac{\pi}{2} R_0, \quad (24)$$

to compare the generalised- k_t variants with Centauro. In the following phenomenological comparisons we quote radii in terms of R_0 . One other notable feature is that Centauro

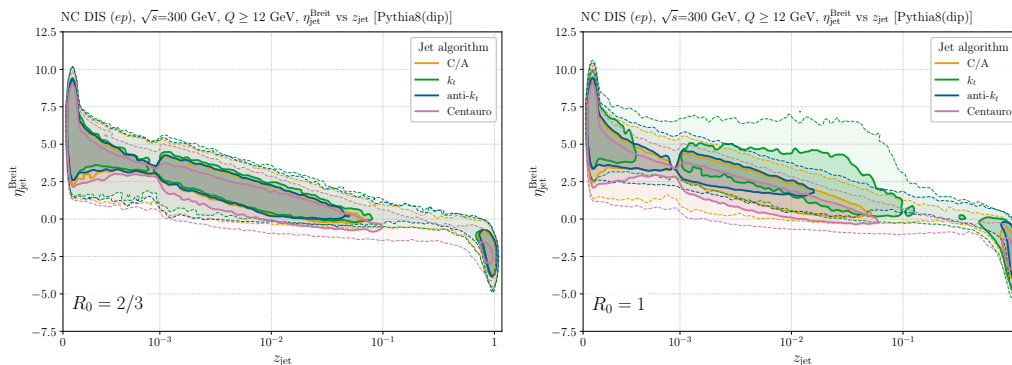


Figure 3: The $z - \eta$ -plane for all jets constructed with the Centauro (pink), C/A (orange), k_t (green) and anti- k_t (blue) algorithms for $R_0 = 2/3$ (left) and $R_0 = 1$ (right), using Eq. (24). The solid (dashed) curves correspond to 68% (95%) of the jets, in terms of their density in the $z - \eta$ -plane.

tends to produce smaller jets with similar-sized jet radius parameter R_0 . This is a consequence of a general property of the Centauro algorithm: it produces comparatively isolated, tight jets. This feature is even more pronounced in the remnant hemisphere, where the size of the jet clusters is much bigger for all variants of the generalised- k_t jet algorithm than for Centauro, which exponentially suppresses clustering of particles in the remnant hemisphere.

Note that for the k_t and C/A variants of the generalised- k_t algorithm, and for Centauro, the exact set of particles clustered into the *macrojet* can change significantly with the choice of R_0 . This occurs because these algorithms cluster particles based on relative softness or angular proximity, so in events with several particles carrying comparable energies, small changes in R_0 can cause different particles to be pulled into or out of the macrojet (as our definition of the macrojet relies on z_{jet}). The anti- k_t variant does not suffer from this, since it always clusters outward from the hardest particle, making the macrojet constituents much more stable against variations in R_0 .

Despite its attractive properties, it is worth pointing out that depending on the choice of R_0 , the anti- k_t variant of our algorithm carries a specific feature. Precisely because it clusters outward from the hardest particle without regard for the hemisphere boundary, it can in principle absorb particles from the remnant hemisphere into the current-hemisphere macrojet. Empirically, values around $R_0 \lesssim 2/3$ are found to significantly reduce contamination of the current-hemisphere macrojet by remnant radiation.

We end this subsection by studying general properties of all jets. Fig. 3 shows the $z - \eta$ plane for all final-state jets constructed with the four algorithms considering 10^6 events. Here, z_{jet} , the lightcone-momentum fraction carried by each of the final-state jets, is defined through Eq. (22) as

$$z_{\text{jet}} = \frac{P \cdot p_{\text{jet}}}{P \cdot q} = \frac{p_{\text{jet}}^E - p_{\text{jet}}^z}{|Q|}, \quad (25)$$

where the last equation holds in the Breit frame. We show contours corresponding to areas that contain 68% (solid) and 95% (dashed) of the total number of jets in the plot, for each of the four considered jet algorithms, and for $R_0 = 2/3$ (left) and $R_0 = 1$ (right).

We observe that the jet algorithms behave relatively similar for $R_0 = 2/3$, where we observe two dense regions: one at small z_{jet} and (large and) positive pseudo-rapidity, and one at large z_{jet} and negative rapidity. The large- z_{jet} region corresponds to the struck quark, whereas the stretched out region in the small- z_{jet} region corresponds to the proton

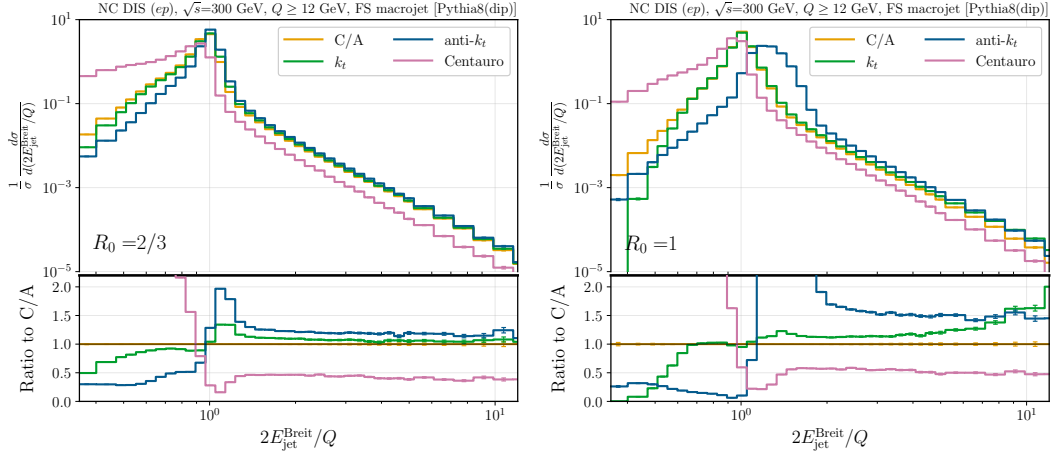


Figure 4: Normalised energy distribution of the final-state macrojet in the Breit frame for the Centauro (pink) jet algorithm, as well as the inclusive versions of the C/A ($p = 0$, orange), k_t ($p = 1$, green) and anti- k_t ($p = -1$, blue) algorithms. We show $R_0 = 2/3$ (left) and $R_0 = 1$ (right).

remnant. We do however notice that our algorithms tend to produce harder (larger z_{jet}) jets than Centauro in the current hemisphere. For $R_0 = 1$, there are larger differences between the algorithms. The central region is populated by soft wide-angle radiation that forms stand-alone jets. It is therefore not surprising that the k_t algorithm yields more jets in this region, as it tends to cluster soft particles first. anti- k_t on the other hand clusters a significant fraction of the partons in the remnant hemisphere with the current hemisphere jets, leading to fewer jets in the remnant hemisphere and harder jets in the current hemisphere. C/A and Centauro seem to be less sensitive to the increased jet radius.

5.2 Macrojet observables at hadron level

We now investigate the properties of the final-state macrojet, identified as the jet that maximises the light-cone component of the original struck quark, as explained in Sec. 4.2. We begin by examining the Breit-frame energy of the macrojet, E_{jet} , normalised to $Q/2$. At the Born-level (in the absence of beam remnants) this variable is exactly 1. The normalised energy distributions of the macrojet for the Centauro (pink), C/A (orange), k_t (green) and anti- k_t (blue) algorithms, with $R_0 = 2/3$ and $R_0 = 1$, are shown in Fig. 4. For both jet radii, the behaviour of the algorithms is very different in the soft region, i.e. for $2E_{\text{jet}}/Q < 1$. Centauro tends to produce a macrojet that is much softer than the other three algorithms. This can be understood by inspecting the distance measure of the Centauro algorithm (cf. Eq. (18)), which effectively prevents partons from clustering in the target hemisphere, and prevents the recoiled struck quark (which may lie at a more central rapidity) from clustering with anything that is not very close in angle. For $R_0 = 2/3$, we observe that the slopes of all four jet algorithms are similar in the hard region, i.e. for $2E_{\text{jet}}/Q > 1$. In the peak region, around $2E_{\text{jet}}/Q \sim 1$, we observe that anti- k_t and k_t shift the peak to slightly larger values compared to C/A, whereas Centauro shifts it to lower values when choosing $R_0 = 2/3$. However, for $R_0 = 1$, we see that the behaviour in the hard region is vastly different for all considered jet algorithms. In particular, all generalised- k_t variants result in a peak that is broader for $R_0 = 1$ with respect to using $R_0 = 2/3$. On the contrary, Centauro shows a peak that is narrower. We stress again

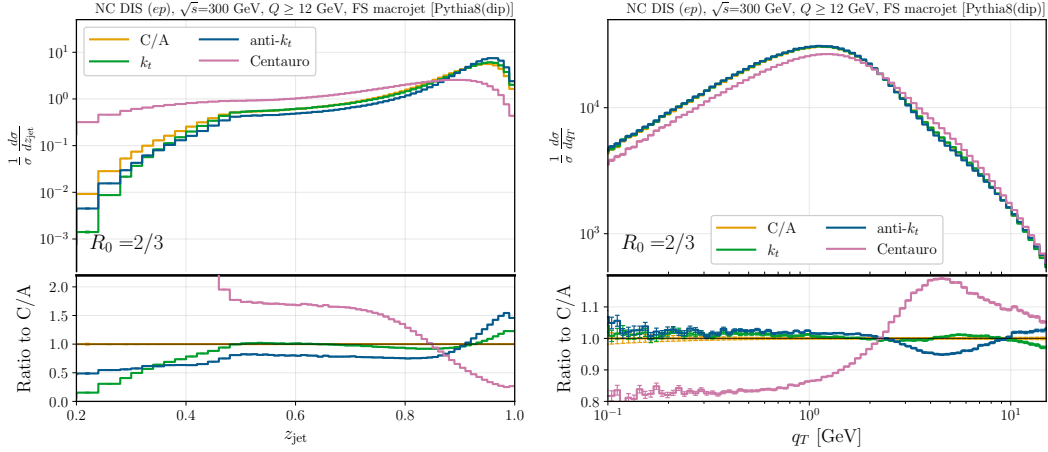


Figure 5: Similar to Fig. 4, but for z_{jet} (left) and q_T (right, see Eq. (26)) with $R_0 = 2/3$.

that for $R_0 = 1$, the anti- k_t variant will have the tendency to contaminate the final-state macrojet with beam radiation.

To further investigate the behaviour of soft radiation, we examine z_{jet} (cf. Eq. (25)). The resulting distributions are shown in the left panel of Fig. 5. One can notice the presence of three regions:

- a peak region, around $z_{\text{jet}} \sim 0.95$, characterised by only soft and collinear emissions;
- a “dijet” region, with $0.5 < z_{\text{jet}} \lesssim 0.7$, where the final-state macrojet still carries most of the original momentum, but a non-negligible fraction has been distributed to other jets;
- a “multi-jet” region, with $z_{\text{jet}} < 0.5$, where the struck quark lost the majority of its energy.

We notice that our generalised- k_t algorithms behave quite similarly in the peak and dijet region, which terminates with a shoulder around $z_{\text{jet}} = 0.5$. This similarity is expected, as these regions are dominated by configurations with at most one hard emission, and the two algorithms behave identically at $\mathcal{O}(\alpha_s)$. Below this shoulder the distributions fall off very quickly. The Centauro algorithm produces a quite different distribution, with the peak region being noticeably smeared towards lower values. The slope of the Centauro distribution agrees with the other three jet algorithms in the dijet region. This is perhaps not surprising, as this is the region that is dominated by two well-separated jets, which means the different treatment of additional soft radiation by the algorithms in their cluster sequences is less impactful. Towards $z_{\text{jet}} \rightarrow 1$, the spectrum differs significantly, which can again be attributed to the behaviour of the $\bar{\eta}$ variable of that algorithm, which prevents some soft radiation carrying away a fraction of the energy from being clustered into the macrojet. Similarly, for $z_{\text{jet}} < 0.5$ the spectrum is dominated by soft jets in the target hemisphere.

The last observable we study is q_T , which is defined as [65]

$$q_T = \frac{|k_T|}{z_{\text{jet}}}, \quad (26)$$

where $|k_T|$ is the modulus of the transverse momentum of the jet in the Breit frame (see Eq. (22)). This observable is known to have little sensitivity to hadronisation, and can

be used to study the transverse momentum distribution of partons inside a proton. We see that all four jet algorithms show a similar slope in the very low- q_T region, but that the three generalised- k_t algorithms result in 20% more events in the region of interest, i.e. $q_T \lesssim Q_{\min}/4 = 3$ GeV.

5.3 Impact of hadronisation and beam remnants

In this section we study the impact of hadronisation and beam remnants on the final-state macrojet. Given the amount of high quality DIS data that currently exists, with more to come from the EIC, it is worth considering if it is possible to use jets to constrain fundamental QCD parameters, like the value of α_s and parameters of various hadronisation models, as is often done with historical e^+e^- collider data and LHC data. Although it is beyond the scope of this paper to carry out a fit of such parameters, we here discuss how one might use the jet algorithms to perform them.

In Fig. 6 we show the normalised energy distribution and lightcone fraction of the final-state macrojet for the Centauro jet algorithm, as well as the inclusive version of our generalised k_t algorithms, for $R_0 = 2/3$.

For each plot we show results at the parton shower level (PS, dotted), parton shower with beam remnants (PS+remn, dashed), and parton shower with beam remnants and hadronisation (PS+remn+hadr, solid). The latter distributions, which also include unstable hadrons decay, coincide with the ones shown in the previous section. We remind the reader, that unlike in hadron-hadron collisions, there is no underlying event in DIS.

Starting with the normalised energy fraction we see that the beam remnants do not contaminate the jet spectra much when compared to the parton level results, although there is some distortion to the right of the peak. The hadronisation, on the other hand, has a larger effect. To the left of the peak, i.e. the soft region, we observe the expected large distortions for all algorithms. To the right of the peak, the normalisation for the three generalised- k_t algorithms is surprisingly insensitive to hadronisation. Centauro receives very large corrections of $\mathcal{O}(50\%)$ here, but the ratio is rather flat, so we attribute the large shift to the normalisation of the plots.

Turning now to the lightcone component z_{jet} we see again that the beam remnants have very little effect on the plots, except for z_{jet} close to 1. Hadronisation on the other hand has once again a large effect, which induces shape differences to be found across all the spectrum, except for just above $z_{\text{jet}} = 0.5$. We also notice that for all jet algorithms, the peak at $z_{\text{jet}} \approx 1$ present at parton level moves at lower values. This observable can be used to constrain both perturbative and non-perturbative parameters. The region $0.65 < z_{\text{jet}} < 0.9$ can be used to fit non-perturbative models. On the other hand, the region just above the shoulder, $0.5 < z_{\text{jet}} < 0.65$, is more insensitive to hadronisation effects and could be used to determine α_s by the comparison of data to predictions.

The last observable we show is q_T , cf. Eq. (26). Contrary to the previously discussed observables, here we see that the hadronisation has relatively little impact compared to the addition of beam remnants. As said before, the transverse momentum distribution of partons in the proton may be studied using this observable, as can be clearly seen from these results. For the generalised- k_t algorithms we see again that more events enter the region of interest ($q_T \lesssim 3$) compared to the Centauro algorithm. Finally we note that the parton-shower only results are not fully physical, which shows itself through kinks at low q_T , which are associated with various shower cut offs.

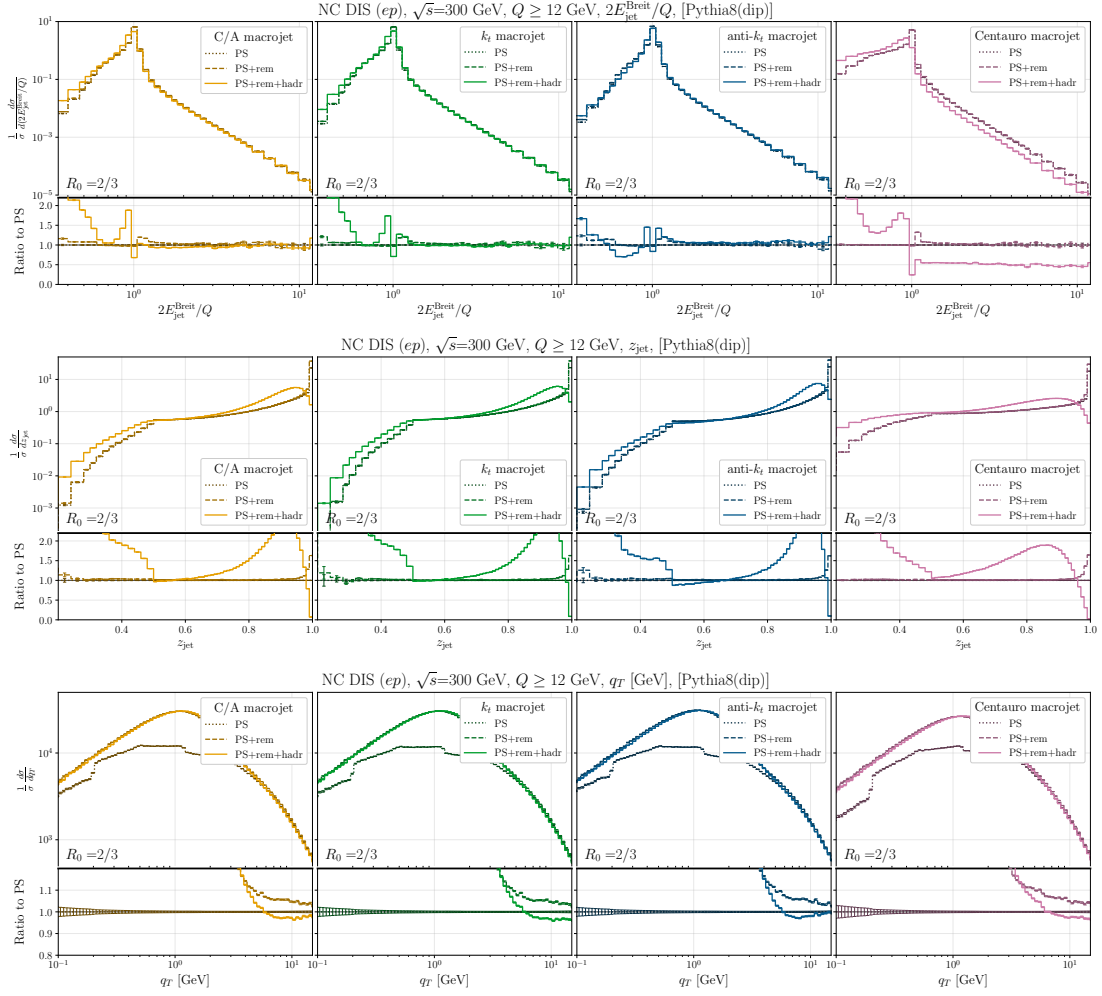


Figure 6: Normalised energy (first row), z_{jet} (second row) and q_T (third row) distributions of the final-state macrojet in the Breit frame for the C/A (first column), k_t (second column), anti- k_t (third column), and Centauro (fourth column) jet algorithms, with $R_0 = 2/3$. We show results at the parton shower level (labeled PS, dotted), parton shower with beam remnants (labeled PS+remn, dashed), and parton shower with beam remnants and hadronisation (labeled PS+remn+hadr, solid).

6 Conclusion

In this paper we have presented a generalisation of the angular-ordered jet algorithm which was first presented in Ref. [8]. The generalisation follows the idea of introducing an exponent to control how much to weight the energy of each pseudojet in the clustering, providing a tunable p -family familiar from similar lepton- and hadron-collider algorithms. The algorithm is very simple, and gives jets that are naturally separated in the current and target hemispheres. We also compared the angular-ordered, k_t and anti- k_t variants of our new inclusive algorithm to the recently-proposed Centauro jet algorithm. One application that we have in mind is to use the generalised k_t algorithms to re-analyse HERA data, with the aim of providing complementary constraints on α_s from jets, and of constraining hadronisation and intrinsic k_t parameters in event generators. Whereas an α_s extraction is unlikely to be competitive with other extractions on its own, we think

there is value in studying non-perturbative physics in DIS data. This is in part due to the fact that DIS allows for studying jets in bins of Q . This could provide a natural handle on the energy dependence of non-perturbative parameters. We leave this to future studies. The algorithm has been implemented as the `DISGenkt` plugin to FASTJET as part of `fjcontrib`.

Acknowledgments

We thank Gavin Salam and Gregory Soyez for useful discussions regarding differences between the Centauro and the generalised k_t jet algorithms. In particular, we thank Gavin Salam for useful discussions on the formulation of the anti- k_t variant presented here. This research was supported by the Italian Ministry of Universities and Research (MUR) under the FIS grant (CUP: D53C24005480001, FLAME) (SFR) and by the Dutch Research Council (NWO) under project number VI.Veni.232.190 (MvB). DP was supported by the Science and Technology Facilities Council (STFC) under the Studentship Grant ST/X508822/1 and is grateful for the hospitality of the CERN TH Department while this research was carried out. AK acknowledges funding from a Royal Society Research Professorship (grant RP\R\231001), and acknowledges the CERN TH Department for hospitality while this research was being carried out.

References

- [1] I. Abt *et al.*, *Measurement of jet production in deep inelastic scattering and NNLO determination of the strong coupling at ZEUS*, Eur. Phys. J. C **83**(11), 1082 (2023), doi:[10.1140/epjc/s10052-023-12180-9](https://doi.org/10.1140/epjc/s10052-023-12180-9), [2309.02889](https://arxiv.org/abs/2309.02889).
- [2] V. Andreev *et al.*, *Unbinned deep learning jet substructure measurement in high Q^2 ep collisions at HERA*, Phys. Lett. B **844**, 138101 (2023), doi:[10.1016/j.physletb.2023.138101](https://doi.org/10.1016/j.physletb.2023.138101), [2303.13620](https://arxiv.org/abs/2303.13620).
- [3] I. Abt *et al.*, *The azimuthal correlation between the leading jet and the scattered lepton in deep inelastic scattering at HERA*, Eur. Phys. J. C **84**(12), 1334 (2024), doi:[10.1140/epjc/s10052-024-13547-2](https://doi.org/10.1140/epjc/s10052-024-13547-2), [2406.01430](https://arxiv.org/abs/2406.01430).
- [4] V. Andreev *et al.*, *Observation and differential cross section measurement of neutral current DIS events with an empty hemisphere in the Breit frame*, Eur. Phys. J. C **84**(7), 720 (2024), doi:[10.1140/epjc/s10052-024-13003-1](https://doi.org/10.1140/epjc/s10052-024-13003-1), [2403.08982](https://arxiv.org/abs/2403.08982).
- [5] V. Andreev *et al.*, *Measurement of the 1-jettiness event shape observable in deep-inelastic electron-proton scattering at HERA*, Eur. Phys. J. C **84**(8), 785 (2024), doi:[10.1140/epjc/s10052-024-13115-8](https://doi.org/10.1140/epjc/s10052-024-13115-8), [2403.10109](https://arxiv.org/abs/2403.10109).
- [6] V. Andreev *et al.*, *Measurement of groomed event shape observables in deep-inelastic electron-proton scattering at HERA*, Eur. Phys. J. C **84**(7), 718 (2024), doi:[10.1140/epjc/s10052-024-12987-0](https://doi.org/10.1140/epjc/s10052-024-12987-0), [2403.10134](https://arxiv.org/abs/2403.10134).
- [7] M. Arratia, Y. Makris, D. Neill, F. Ringer and N. Sato, *Asymmetric jet clustering in deep-inelastic scattering*, Phys. Rev. D **104**(3), 034005 (2021), doi:[10.1103/PhysRevD.104.034005](https://doi.org/10.1103/PhysRevD.104.034005), [2006.10751](https://arxiv.org/abs/2006.10751).

- [8] M. van Beekveld and S. Ferrario Ravasio, *Next-to-leading-logarithmic PanScales showers for Deep Inelastic Scattering and Vector Boson Fusion*, JHEP **02**, 001 (2024), doi:[10.1007/JHEP02\(2024\)001](https://doi.org/10.1007/JHEP02(2024)001), [2305.08645](https://arxiv.org/abs/2305.08645).
- [9] P. Caucal, E. Iancu, A. H. Mueller and F. Yuan, *Jet Definition and Transverse-Momentum-Dependent Factorization in Semi-inclusive Deep-Inelastic Scattering*, Phys. Rev. Lett. **134**(6), 061903 (2025), doi:[10.1103/PhysRevLett.134.061903](https://doi.org/10.1103/PhysRevLett.134.061903), [2408.03129](https://arxiv.org/abs/2408.03129).
- [10] Y. Makris, *Revisiting the role of grooming in DIS*, Phys. Rev. D **103**(5), 054005 (2021), doi:[10.1103/PhysRevD.103.054005](https://doi.org/10.1103/PhysRevD.103.054005), [2101.02708](https://arxiv.org/abs/2101.02708).
- [11] M. Knobbe, D. Reichelt and S. Schumann, *(N)NLO+NLL' accurate predictions for plain and groomed 1-jettiness in neutral current DIS*, JHEP **09**, 194 (2023), doi:[10.1007/JHEP09\(2023\)194](https://doi.org/10.1007/JHEP09(2023)194), [2306.17736](https://arxiv.org/abs/2306.17736).
- [12] S. Fang, M.-S. Gao, H. T. Li and D. Y. Shao, *$N^3LL + \mathcal{O}(\alpha_s^2)$ predictions of lepton-jet azimuthal angular distribution in deep-inelastic scattering*, JHEP **01**, 029 (2025), doi:[10.1007/JHEP01\(2025\)029](https://doi.org/10.1007/JHEP01(2025)029), [2409.09248](https://arxiv.org/abs/2409.09248).
- [13] H. Cao, Z.-B. Kang, X. Liu and S. Mantry, *One-jettiness DIS event shape at $N^3LL + \mathcal{O}(\alpha_s^2)$* , Phys. Rev. D **110**(1), 014045 (2024), doi:[10.1103/PhysRevD.110.014045](https://doi.org/10.1103/PhysRevD.110.014045), [2401.01941](https://arxiv.org/abs/2401.01941).
- [14] J.-H. Ee, D. Kang, C. Lee and I. W. Stewart, *Precision DIS thrust predictions for HERA and EIC*, JHEP **07**, 240 (2025), doi:[10.1007/JHEP07\(2025\)240](https://doi.org/10.1007/JHEP07(2025)240), [2504.05234](https://arxiv.org/abs/2504.05234).
- [15] M. van Beekveld, L. Buonocore, S. Ferrario Ravasio, P. F. Monni, A. Soto-Ontoso and G. Soyez, *A new suite of Lund-tree observables to resolve jets* (2025), [2511.16723](https://arxiv.org/abs/2511.16723).
- [16] V. Antonelli, M. Dasgupta and G. P. Salam, *Resummation of thrust distributions in DIS*, JHEP **02**, 001 (2000), doi:[10.1088/1126-6708/2000/02/001](https://doi.org/10.1088/1126-6708/2000/02/001), [hep-ph/9912488](https://arxiv.org/abs/hep-ph/9912488).
- [17] M. Dasgupta and G. P. Salam, *Resummation of the jet broadening in DIS*, Eur. Phys. J. C **24**, 213 (2002), doi:[10.1007/s100520200915](https://doi.org/10.1007/s100520200915), [hep-ph/0110213](https://arxiv.org/abs/hep-ph/0110213).
- [18] M. Dasgupta and G. P. Salam, *Event shapes in e^+e^- annihilation and deep inelastic scattering*, J. Phys. G **30**, R143 (2004), doi:[10.1088/0954-3899/30/5/R01](https://doi.org/10.1088/0954-3899/30/5/R01), [hep-ph/0312283](https://arxiv.org/abs/hep-ph/0312283).
- [19] D. Kang, C. Lee and I. W. Stewart, *Using 1-Jettiness to Measure 2 Jets in DIS 3 Ways*, Phys. Rev. D **88**, 054004 (2013), doi:[10.1103/PhysRevD.88.054004](https://doi.org/10.1103/PhysRevD.88.054004), [1303.6952](https://arxiv.org/abs/1303.6952).
- [20] Z.-B. Kang, X. Liu and S. Mantry, *1-jettiness DIS event shape: NNLL+NLO results*, Phys. Rev. D **90**(1), 014041 (2014), doi:[10.1103/PhysRevD.90.014041](https://doi.org/10.1103/PhysRevD.90.014041), [1312.0301](https://arxiv.org/abs/1312.0301).
- [21] Z. Chu, Y. Wang, J.-H. Ee, J. Chen and D. Kang, *I-jettiness with jet axis at $O(\alpha_s)$ in deep inelastic scattering*, JHEP **06**, 111 (2022), doi:[10.1007/JHEP06\(2022\)111](https://doi.org/10.1007/JHEP06(2022)111), [2202.08040](https://arxiv.org/abs/2202.08040).
- [22] P. Agostini *et al.*, *The Large Hadron-Electron Collider at the HL-LHC*, J. Phys. G **48**(11), 110501 (2021), doi:[10.1088/1361-6471/abf3ba](https://doi.org/10.1088/1361-6471/abf3ba), [2007.14491](https://arxiv.org/abs/2007.14491).
- [23] A. Accardi *et al.*, *Electron Ion Collider: The Next QCD Frontier: Understanding the glue that binds us all*, Eur. Phys. J. A **52**(9), 268 (2016), doi:[10.1140/epja/i2016-16268-9](https://doi.org/10.1140/epja/i2016-16268-9), [1212.1701](https://arxiv.org/abs/1212.1701).

- [24] R. Abdul Khalek *et al.*, *Science Requirements and Detector Concepts for the Electron-Ion Collider: EIC Yellow Report*, Nucl. Phys. A **1026**, 122447 (2022), doi:[10.1016/j.nuclphysa.2022.122447](https://doi.org/10.1016/j.nuclphysa.2022.122447), [2103.05419](https://arxiv.org/abs/2103.05419).
- [25] M. Cacciari, G. P. Salam and G. Soyez, *The anti- k_t jet clustering algorithm*, JHEP **04**, 063 (2008), doi:[10.1088/1126-6708/2008/04/063](https://doi.org/10.1088/1126-6708/2008/04/063), [0802.1189](https://arxiv.org/abs/0802.1189).
- [26] S. Catani, Y. L. Dokshitzer and B. R. Webber, *The k_\perp clustering algorithm for jets in deep inelastic scattering and hadron collisions*, Phys. Lett. B **285**, 291 (1992), doi:[10.1016/0370-2693\(92\)91467-N](https://doi.org/10.1016/0370-2693(92)91467-N).
- [27] S. Catani, Y. L. Dokshitzer, M. Olsson, G. Turnock and B. R. Webber, *New clustering algorithm for multi - jet cross-sections in $e^+ e^-$ annihilation*, Phys. Lett. B **269**, 432 (1991), doi:[10.1016/0370-2693\(91\)90196-W](https://doi.org/10.1016/0370-2693(91)90196-W).
- [28] N. Brown and W. J. Stirling, *Finding jets and summing soft gluons: A New algorithm*, Z. Phys. C **53**, 629 (1992), doi:[10.1007/BF01559740](https://doi.org/10.1007/BF01559740).
- [29] M. Wobisch and T. Wengler, *Hadronization corrections to jet cross-sections in deep inelastic scattering*, In *Workshop on Monte Carlo Generators for HERA Physics (Plenary Starting Meeting)*, pp. 270–279 (1998), [hep-ph/9907280](https://arxiv.org/abs/hep-ph/9907280).
- [30] Y. L. Dokshitzer, G. D. Leder, S. Moretti and B. R. Webber, *Better jet clustering algorithms*, JHEP **08**, 001 (1997), doi:[10.1088/1126-6708/1997/08/001](https://doi.org/10.1088/1126-6708/1997/08/001), [hep-ph/9707323](https://arxiv.org/abs/hep-ph/9707323).
- [31] S. D. Ellis and D. E. Soper, *Successive combination jet algorithm for hadron collisions*, Phys. Rev. D **48**, 3160 (1993), doi:[10.1103/PhysRevD.48.3160](https://doi.org/10.1103/PhysRevD.48.3160), [hep-ph/9305266](https://arxiv.org/abs/hep-ph/9305266).
- [32] S. Catani, Y. L. Dokshitzer, M. H. Seymour and B. R. Webber, *Longitudinally invariant K_t clustering algorithms for hadron hadron collisions*, Nucl. Phys. B **406**, 187 (1993), doi:[10.1016/0550-3213\(93\)90166-M](https://doi.org/10.1016/0550-3213(93)90166-M).
- [33] W. Bartel *et al.*, *Experimental Studies on Multi-Jet Production in e^+e^- Annihilation at PETRA Energies*, Z. Phys. C **33**, 23 (1986), doi:[10.1007/BF01410449](https://doi.org/10.1007/BF01410449).
- [34] S. Bethke *et al.*, *Experimental Investigation of the Energy Dependence of the Strong Coupling Strength*, Phys. Lett. B **213**, 235 (1988), doi:[10.1016/0370-2693\(88\)91032-5](https://doi.org/10.1016/0370-2693(88)91032-5).
- [35] M. R. Adams *et al.*, *First measurements of Jet Production Rates in Deep Inelastic Lepton Proton Scattering*, Phys. Rev. Lett. **69**, 1026 (1992), doi:[10.1103/PhysRevLett.69.1026](https://doi.org/10.1103/PhysRevLett.69.1026).
- [36] M. R. Adams *et al.*, *Q^2 dependence of the average squared transverse energy of jets in deep inelastic muon - nucleon scattering with comparison to QCD*, Phys. Rev. Lett. **72**, 466 (1994), doi:[10.1103/PhysRevLett.72.466](https://doi.org/10.1103/PhysRevLett.72.466).
- [37] T. Ahmed *et al.*, *Determination of the strong coupling constant from jet rates in deep inelastic scattering*, Phys. Lett. B **346**, 415 (1995), doi:[10.1016/0370-2693\(95\)00095-3](https://doi.org/10.1016/0370-2693(95)00095-3).
- [38] M. Derrick *et al.*, *Observation of jet production in deep inelastic scattering with a large rapidity gap at HERA*, Phys. Lett. B **332**, 228 (1994), doi:[10.1016/0370-2693\(94\)90883-4](https://doi.org/10.1016/0370-2693(94)90883-4).
- [39] M. Derrick *et al.*, *Measurement of α_s from jet rates in deep inelastic scattering at HERA*, Phys. Lett. B **363**, 201 (1995), doi:[10.1016/0370-2693\(95\)01284-W](https://doi.org/10.1016/0370-2693(95)01284-W), [hep-ex/9510001](https://arxiv.org/abs/hep-ex/9510001).

- [40] S. Aid *et al.*, *Transverse energy and forward jet production in the low x regime at HERA*, Phys. Lett. B **356**, 118 (1995), doi:[10.1016/0370-2693\(95\)00804-T](https://doi.org/10.1016/0370-2693(95)00804-T), [hep-ex/9506012](https://arxiv.org/abs/hep-ex/9506012).
- [41] C. Adloff *et al.*, *Diffractive dijet production at HERA*, Eur. Phys. J. C **6**, 421 (1999), doi:[10.1007/s100529801046](https://doi.org/10.1007/s100529801046), [hep-ex/9808013](https://arxiv.org/abs/hep-ex/9808013).
- [42] C. Adloff *et al.*, *Measurement of internal jet structure in dijet production in deep inelastic scattering at HERA*, Nucl. Phys. B **545**, 3 (1999), doi:[10.1016/S0550-3213\(99\)00118-2](https://doi.org/10.1016/S0550-3213(99)00118-2), [hep-ex/9901010](https://arxiv.org/abs/hep-ex/9901010).
- [43] C. Adloff *et al.*, *Forward jet and particle production at HERA*, Nucl. Phys. B **538**, 3 (1999), doi:[10.1016/S0550-3213\(98\)00745-7](https://doi.org/10.1016/S0550-3213(98)00745-7), [hep-ex/9809028](https://arxiv.org/abs/hep-ex/9809028).
- [44] C. Adloff *et al.*, *Measurement and QCD analysis of jet cross-sections in deep inelastic positron - proton collisions at \sqrt{s} of 300 GeV*, Eur. Phys. J. C **19**, 289 (2001), doi:[10.1007/s100520100621](https://doi.org/10.1007/s100520100621), [hep-ex/0010054](https://arxiv.org/abs/hep-ex/0010054).
- [45] C. Adloff *et al.*, *Measurement of inclusive jet cross-sections in deep inelastic ep scattering at HERA*, Phys. Lett. B **542**, 193 (2002), doi:[10.1016/S0370-2693\(02\)02375-4](https://doi.org/10.1016/S0370-2693(02)02375-4), [hep-ex/0206029](https://arxiv.org/abs/hep-ex/0206029).
- [46] S. Chekanov *et al.*, *Inclusive jet cross-sections in the Breit frame in neutral current deep inelastic scattering at HERA and determination of α_s* , Phys. Lett. B **547**, 164 (2002), doi:[10.1016/S0370-2693\(02\)02763-6](https://doi.org/10.1016/S0370-2693(02)02763-6), [hep-ex/0208037](https://arxiv.org/abs/hep-ex/0208037).
- [47] S. Chekanov *et al.*, *An NLO QCD analysis of inclusive cross-section and jet-production data from the zeus experiment*, Eur. Phys. J. C **42**, 1 (2005), doi:[10.1140/epjc/s2005-02293-x](https://doi.org/10.1140/epjc/s2005-02293-x), [hep-ph/0503274](https://arxiv.org/abs/hep-ph/0503274).
- [48] S. Chekanov *et al.*, *Inclusive-jet and dijet cross-sections in deep inelastic scattering at HERA*, Nucl. Phys. B **765**, 1 (2007), doi:[10.1016/j.nuclphysb.2006.09.018](https://doi.org/10.1016/j.nuclphysb.2006.09.018), [hep-ex/0608048](https://arxiv.org/abs/hep-ex/0608048).
- [49] A. Aktas *et al.*, *Measurement of inclusive jet production in deep-inelastic scattering at high Q^2 and determination of the strong coupling*, Phys. Lett. B **653**, 134 (2007), doi:[10.1016/j.physletb.2007.07.050](https://doi.org/10.1016/j.physletb.2007.07.050), [0706.3722](https://arxiv.org/abs/0706.3722).
- [50] F. D. Aaron *et al.*, *Jet Production in ep Collisions at High Q^2 and Determination of α_s* , Eur. Phys. J. C **65**, 363 (2010), doi:[10.1140/epjc/s10052-009-1208-7](https://doi.org/10.1140/epjc/s10052-009-1208-7), [0904.3870](https://arxiv.org/abs/0904.3870).
- [51] F. D. Aaron *et al.*, *Jet Production in ep Collisions at Low Q^2 and Determination of α_s* , Eur. Phys. J. C **67**, 1 (2010), doi:[10.1140/epjc/s10052-010-1282-x](https://doi.org/10.1140/epjc/s10052-010-1282-x), [0911.5678](https://arxiv.org/abs/0911.5678).
- [52] V. Andreev *et al.*, *Measurement of multijet production in ep collisions at high Q^2 and determination of the strong coupling α_s* , Eur. Phys. J. C **75**(2), 65 (2015), doi:[10.1140/epjc/s10052-014-3223-6](https://doi.org/10.1140/epjc/s10052-014-3223-6), [1406.4709](https://arxiv.org/abs/1406.4709).
- [53] F. A. Dreyer, G. P. Salam and G. Soyez, *The Lund Jet Plane*, JHEP **12**, 064 (2018), doi:[10.1007/JHEP12\(2018\)064](https://doi.org/10.1007/JHEP12(2018)064), [1807.04758](https://arxiv.org/abs/1807.04758).
- [54] M. Cacciari, G. P. Salam and G. Soyez, *FastJet User Manual*, Eur. Phys. J. C **72**, 1896 (2012), doi:[10.1140/epjc/s10052-012-1896-2](https://doi.org/10.1140/epjc/s10052-012-1896-2), [1111.6097](https://arxiv.org/abs/1111.6097).
- [55] B. R. Webber, *Factorization and jet clustering algorithms for deep inelastic scattering*, J. Phys. G **19**, 1567 (1993), doi:[10.1088/0954-3899/19/10/012](https://doi.org/10.1088/0954-3899/19/10/012).

- [56] G. Breit, *The Effect of Retardation on the Interaction of Two Electrons*, Phys. Rev. **34**, 553 (1929), doi:[10.1103/PhysRev.34.553](https://doi.org/10.1103/PhysRev.34.553).
- [57] F. J. Ernst, R. G. Sachs and K. C. Wali, *Electromagnetic form factors of the nucleon*, Phys. Rev. **119**, 1105 (1960), doi:[10.1103/PhysRev.119.1105](https://doi.org/10.1103/PhysRev.119.1105).
- [58] R. G. Sachs, *High-Energy Behavior of Nucleon Electromagnetic Form Factors*, Phys. Rev. **126**, 2256 (1962), doi:[10.1103/PhysRev.126.2256](https://doi.org/10.1103/PhysRev.126.2256).
- [59] R. Devenish and A. Cooper-Sarkar, *Deep inelastic scattering*, doi:[10.1093/acprof:oso/9780198506713.001.0001](https://doi.org/10.1093/acprof:oso/9780198506713.001.0001) (2004).
- [60] C. Bierlich *et al.*, *A comprehensive guide to the physics and usage of PYTHIA 8.3*, SciPost Phys. Codeb. **2022**, 8 (2022), doi:[10.21468/SciPostPhysCodeb.8.2203.11601](https://doi.org/10.21468/SciPostPhysCodeb.8.2203.11601).
- [61] B. Cabouat and T. Sjöstrand, *Some Dipole Shower Studies*, Eur. Phys. J. C **78**(3), 226 (2018), doi:[10.1140/epjc/s10052-018-5645-z](https://doi.org/10.1140/epjc/s10052-018-5645-z), [1710.00391](https://arxiv.org/abs/1710.00391).
- [62] C. Bierlich *et al.*, *Robust Independent Validation of Experiment and Theory: Rivet version 3*, SciPost Phys. **8**, 026 (2020), doi:[10.21468/SciPostPhys.8.2.026](https://doi.org/10.21468/SciPostPhys.8.2.026), [1912.05451](https://arxiv.org/abs/1912.05451).
- [63] P. Skands, S. Carrazza and J. Rojo, *Tuning PYTHIA 8.1: the Monash 2013 Tune*, Eur. Phys. J. C **74**(8), 3024 (2014), doi:[10.1140/epjc/s10052-014-3024-y](https://doi.org/10.1140/epjc/s10052-014-3024-y), [1404.5630](https://arxiv.org/abs/1404.5630).
- [64] M. Cacciari, G. P. Salam and G. Soyez, *The Catchment Area of Jets*, JHEP **04**, 005 (2008), doi:[10.1088/1126-6708/2008/04/005](https://doi.org/10.1088/1126-6708/2008/04/005), [0802.1188](https://arxiv.org/abs/0802.1188).
- [65] P. J. Mulders and R. D. Tangerman, *The Complete tree level result up to order $1/Q$ for polarized deep inelastic lepton production*, Nucl. Phys. B **461**, 197 (1996), doi:[10.1016/0550-3213\(95\)00632-X](https://doi.org/10.1016/0550-3213(95)00632-X), [Erratum: Nucl.Phys.B 484, 538–540 (1997)], [hep-ph/9510301](https://arxiv.org/abs/hep-ph/9510301).